UDC 539.22:539.12:548.4

*Abhay P. Srivastava [a], Anod Kumar Singh [b], Reetesh Srivastava [c], Harish Chandra Srivastava [d]*

# EXPLORING THE PHYSICAL PROPERTIES OF $Al_2O_3$ UNDER PRESSURE: A STUDY UTILIZING DFT AND EQUATION OF STATE METHODS

**[a] Department of Humanities and Applied Science, Bansal Institute of Engineering and Technology, Lucknow (UP), India**
**[b] Department of Humanities and Applied Science, School of Management Sciences, Lucknow (UP), India**
**[c] Department of Physics, Nandini Nagar P.G. College, Nawabganj, Gonda (UP), India**
**[d] Munna Lal Inter College, Wazirganj, Budaun (UP), India**

Using first-principles density functional theory (DFT) calculations in conjunction with the Murnaghan and Srivastava–Pandey equations of state (EOS), we comprehensively investigate the effect of pressure on the structural, mechanical, thermal, and optical properties of aluminum oxide ($Al_2O_3$). Based on structural optimization, we confirm the stability of the corundum phase up to 100 GPa; we find a 10–15% decrease in volume, and the bulk modulus increases from 253 GPa to 330 GPa. The band gap decreases from 9.9 eV to 8.2 eV with rising pressure, as electronic overlap increases and the optical absorption spectrum is likely to be redshifted; the bulk, shear, and Weng's moduli also increase, indicating greater incompressibility. Meanwhile, the thermal conductivity also increases slightly from 30 W/m·K to 37.7 W/m·K, which can be attributed to the increasing phonon scattering. Optical results reveal a redshift of the absorption edge and a pressure-sensitive refractive index in the 4–6 eV range. The agreement between DFT predictions and experimental results further confirms the model's accuracy. This consistency supports the feasibility of $Al_2O_3$ for optoelectronic and geophysical applications at high pressure and provides new insights into its electronic and optical response under pressure.

**Keywords**: density functional theory, $Al_2O_3$, electronic properties, optical properties, pressure.

**DOI:** 10.32434/0321-4095-2026-168-5-137-149

## *Introduction*

Alumina, or aluminum oxide ($Al_2O_3$), has been a highly versatile material for many years, offering scientific value as well as industrial utility. It has these great physical and chemical properties. It is highly tough and thermally stable, with a wide bandgap and good dielectric strength. Therefore, we encounter $Al_2O_3$ in various applications, including electronics, optics, protective coatings, and catalysis [1,2].

We found its ultraviolet-infrared transparency and high electrical resistivity particularly interesting. Thus, these properties make it suitable for use as an insulating layer in microelectronics, optical windows, and ultra-sensitive thin-film device substrates. Therefore, we should explore the fundamental electrical and optical properties of alumina, particularly its interactions with the environment, to optimize its applications [3,4]. Now, consider pressure and how it

© Abhay P. Srivastava, Anod Kumar Singh, Reetesh Srivastava, Harish Chandra Srivastava, 2026

This article is an open access article distributed under the terms and conditions of the Creative Commons Attribution (CC BY) license (https://creativecommons.org/licenses/by/4.0/).

alters a material. Under increased pressure, it can alter the crystal structure, electronic band formation, and optical properties.

If we consider alumina itself [5], hydrostatic pressure can uniquely alter its interfacial structure with the atoms it interacts with, and these atoms have different electronic states and dielectric properties. These shifts might affect electrical conductivity, light absorption, and light emission. If we are devising components that must operate at extreme pressures, such as high-pressure sensors or geophysical tools, we need to understand what happens under pressure [6,7].

Another concern is that, despite what we know about alumina under normal conditions, we still have little idea what it will do under high pressure. Some of us have obtained conflicting results because these experiments are high-pressure and alumina exists in various forms [8,9]. Thus, computational procedures such as DFT are particularly appealing. Using DFT, we developed materials from first principles and determined their responses to force with much less reliance on actual data [10–12].

As they can be used in applications such as band structure, dielectric function, and optical absorption, DFT calculations are suitable for several properties, such as band structure and dielectric function under the influence of pressure, that is, to provide, for example, our experiments, which contribute to new materials [13–16].

To this end, we are applying density functional theory (DFT) to investigate the role of hydrostatic pressure on the electrical and optical properties of $Al_2O_3$. We will better characterize the pressure-dependent electrical and optical properties of $Al_2O_3$ by measuring the bandgap, density of states, dielectric function, and optical absorption. We anticipate that this work will lead to more pressure-tunable materials, as well as advanced electronics and photonics that can operate effectively even in hostile applications.

***Computational methodology***

We used a first-principles approach to explore a material's pressure sensitivity using Density Functional Theory (DFT). We used the Vienna Ab initio Simulation Package (VASP) for testing. We mainly accounted for exchange-correlation effects using the Generalized Gradient Approximation (GGA) with the Perdew, Burke, and Ernzerhof (PBE) functional [17–19].

To facilitate the procedure, we used Projector Augmented-Wave (PAW) potentials. For accurate calculations, we used a plane-wave energy cutoff of 500 eV and an 8×8×8 Monkhorst-Pack k-point mesh for reliable convergence. We systematically calculated the effects of increasing pressure by adding hydrostatic pressure in increments of 0, 20, 40, 60, 80, and 100 GPa [20]. Under these conditions, we examined the effects of the physical parameters: lattice, electronic band gap, elastic constants, thermal conductivity (calculated from phonon dispersion calculations), and complex dielectric function [21].

These studies provided information on the material's structure and its electronic, mechanical, thermal, and optical performance under extreme stress. All simulations were performed in a static lattice at 300 K, or the system's ground state [22]. This allowed us to identify pressure-induced changes in the material's structure, mechanical, and electronic properties without thermal effects. For our comparisons, we rely on experimental data from the literature, commonly collected at about 300 K, which serve as an effective and practical benchmark for comparing theoretical and experimental findings [23,24].

***Results and discussion***

*Structural properties under pressure*

Alumina, better known as aluminum oxide ($Al_2O_3$), typically forms corundum with a trigonal crystal system (R-3c space group). The aluminum (Al) atoms, apparently, nest near each other in a hexagonal close-packed arrangement of oxygen atoms (O), forming distorted $AlO_6$ octahedra. Imagine the four atoms of aluminum surrounding each oxygen atom, a nice sort of symmetry. Interesting changes take place in $Al_2O_3$. As pressure increases, intriguing changes in $Al_2O_3$ structures are observed (Fig. 1).

Volume decreases as the unit-cell atoms are compressed, pushing them closer together into a more compact structure as they are squeezed into smaller units under atomic pressure. This proximity increases atomic interaction, and the material's behavior changes under strain. A shorter Al–O bond length creates a denser structure, and overall, the material is denser. Although the corundum form tends to be stable, the atomic arrangement varies with external pressure and accordingly affects its electronic and mechanical properties, while remaining stable.

Aluminum oxide undergoes the $\alpha$-$Al_2O_3$ form at standard ambient pressure (0 GPa), with the values of the lattice parameters measuring only about a=4.76 Å, c≈12.99 Å. For the bonds, the Al–O link lengths are around 1.85–1.97 Å, but at 50 GPa the shape compresses slightly, especially along the a-axis. So, Al–O bonds are around 1.75/1.90 Å, and the total volume decreases by about 10–15%. The material does surprisingly respond. Finally, high pressures (around 100 GPa) could convert $\alpha$-$Al_2O_3$ into a metastable phase, which could evolve to become a higher-density $Rh_2O_3$(II)-type or possibly $CaIrO_3$-type when bond lengths reach just 1.65 Å to

1.80 Å (the reaction also shows an increase in volume), which, at higher pressures, gives a higher density and a harder bond structure.

Figure 2 shows the variation of the DFT-optimized unit-cell volume of $Al_2O_3$ as a function of applied hydrostatic pressure from 0 to 100 GPa. The volume decreases continuously and monotonically with increasing pressure, from around 108 $Å^3$ at 0 GPa to 80 $Å^3$ at 100 GPa, a decrease of about 26%.

This volume decrease directly results from compressing the crystal lattice under hydrostatic pressure. At low pressures, the volume decreases more

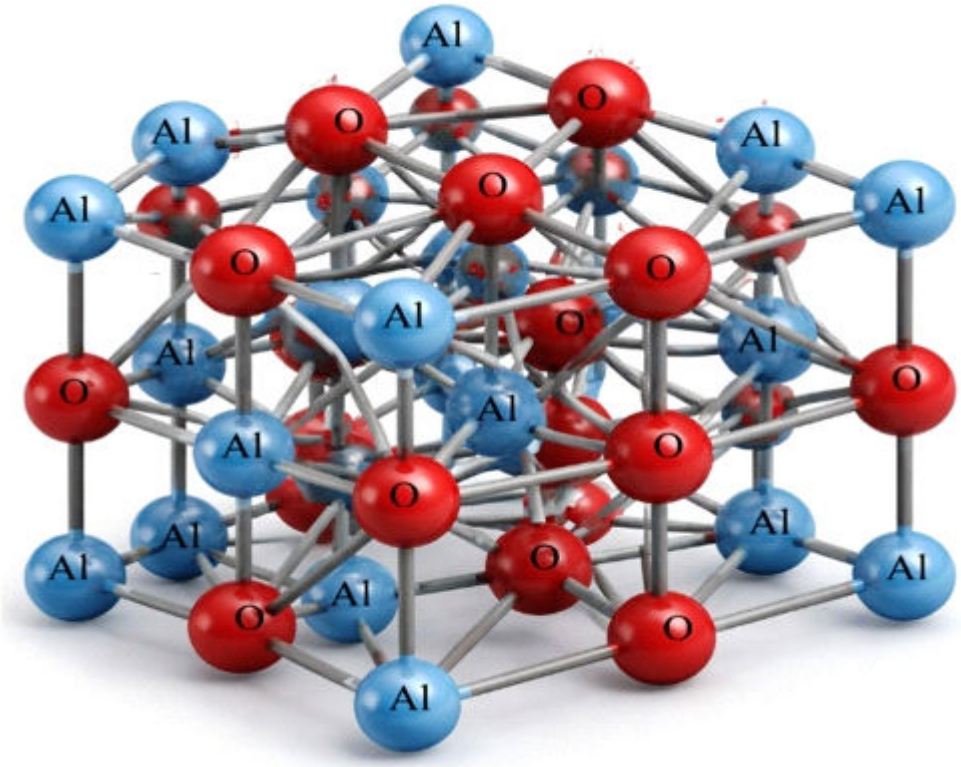



Fig. 1. 3D structural image of $Al_2O_3$ optimized by DFT

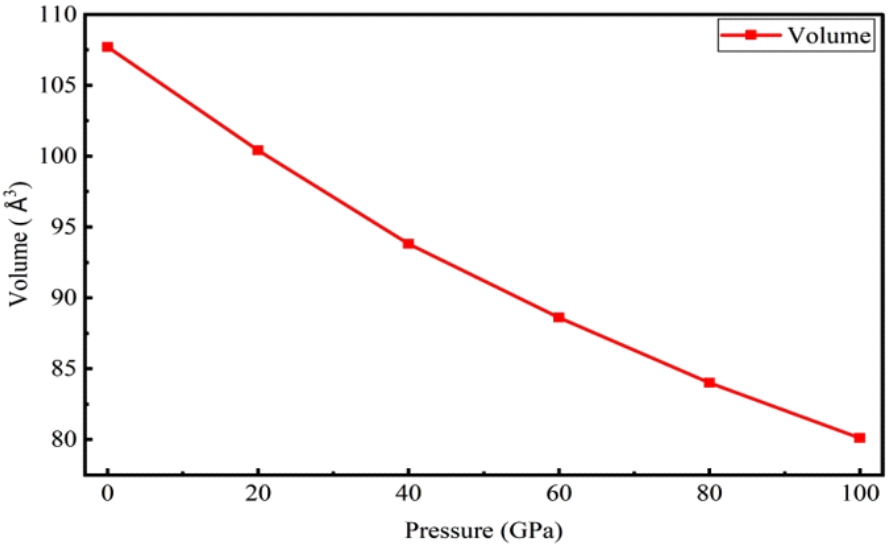



Fig. 2. Variation of volume with respect to pressure optimized by DFT of $Al_2O_3$

quickly because interatomic distances can be reduced with comparatively little resistance. As pressure increases, the slope of the volume–pressure curve decreases. This nonlinear behavior indicates that $Al_2O_3$ becomes progressively less compressible at high pressures, as short-range repulsive interactions between neighboring atoms become increasingly important.

The smooth variation of volume over the entire pressure range suggests a normal structural response to compression. In particular, the absence of abrupt discontinuities or anomalous changes in the volume–pressure curve indicates no obvious first-order pressure-induced structural transition from the volume data alone up to 100 GPa. However, structural or dynamical stability should also be considered, such as enthalpy comparisons between competing phases or phonon calculations. Overall, the pressure-induced volume contraction is consistent with that of a mechanically compressed solid and provides a basis for investigating the elastic, electronic, vibrational, and optical properties of $Al_2O_3$.

*Electronic properties*

Figure 3 illustrates how a material's band gap energy changes with increasing pressure, based on computer models (Density Functional Theory, or DFT) and experimental data [25,26]. From 0 to 100 GPa, increasing pressure on the material continuously decreases the band gap energy. Under pressure, the electronic band structure appears to compress. At 0 GPa, however, both DFT calculations give band gap values around 9.8 eV, which are close.

However, the DFT values seem lower than experimental values. Pressure is commonly used to compress materials and reduce atomic spacing, allowing electrons to interact more and narrowing the energy difference between specific bands. On the other hand, the close agreement between the DFT predictions and the experimental results suggests that our models are highly accurate. They only differ marginally because DFT has limitations in predicting absolute band gap values. This means that the electronic properties of a material are compressed. This small band gap under strain indicates electron interactions, which are important to the material's structure.

*Mechanical properties*

Table summarizes the pressure-dependent mechanical properties of $Al_2O_3$ (Bulk modulus, Shear modulus, Weng's modulus, and Poisson's ratio) (0–100 GPa) and compares DFT-derived Bulk modulus estimates with experimental results [22]. During the experiment, the bulk modulus increased from 253 GPa at 0 GPa to 330 GPa at 100 GPa, indicating how resistance to volume compression increases under pressure. This is because interatomic forces increase, and the material's compressibility decreases with pressure. In addition, as pressure increases, the shear modulus rises from 170 GPa to 220 GPa, confirming improved deformation behavior. Weng's modulus increases from 410 GPa at ambient to 515 GPa at 100 GPa, likely due to greater pressure sensitivity. The increase in the three elastic moduli (B, G, and E) is consistent with the rise in pressure. At high pressure, $Al_2O_3$ shows higher mechanical strength and structural stability, as is usually observed for harder ceramic materials. Poisson's ratio drops slightly with increasing pressure, from 0.22 to 0.20.

This reduction indicates a gradual, linear progression toward more directional, or less ductile, joint-binding properties, as well as more brittle material at high pressure. The low Poisson's ratio

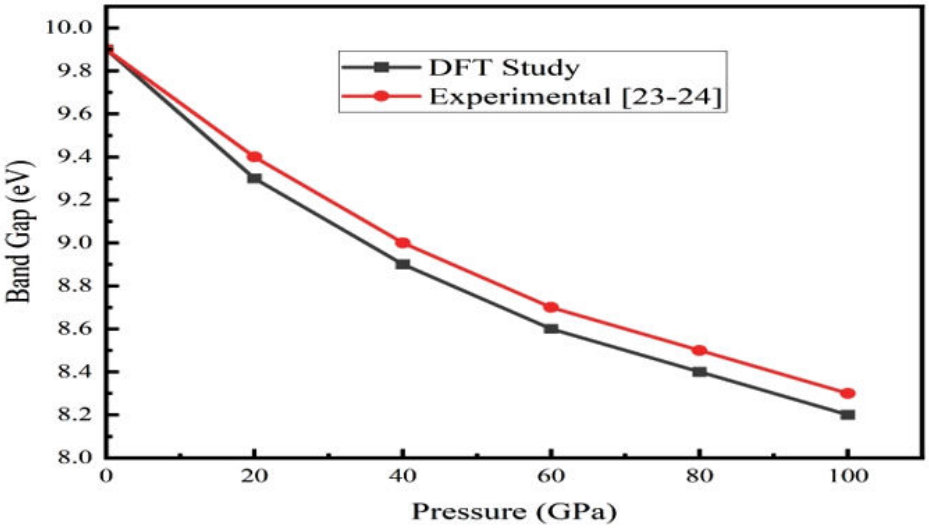



Fig. 3. Variation of band gap vs. pressure for $Al_2O_3$ by DFT and experiment [25,26]

values also confirm strong covalent–ionic bonding in $Al_2O_3$ and its resistance to shear deformation. In contrast to the bulk modulus values from experiment [22], DFT and measurements at lower pressures (0 and 20 GPa) agree well. At higher pressures, the difference is minimal, and the DFT values are slightly greater than the experimental values (330 GPa and 320 GPa at 100 GPa, respectively).

This slight overestimation is consistent with the GGA-PBE standard, where the stiffness curve slightly exceeds the experimental values. However, despite this deviation, it remains close to acceptable values, so the computational approach is likely accurate and reliable. Overall, Table shows that $Al_2O_3$ achieves improved stiffness, strength, and resistance to volumetric and shear deformation under elevated pressure and exhibits widely accepted behavior consistent with experimental reports [22]. These values suggest applicability to applications requiring high mechanical properties, such as protective coatings, structural ceramics, and high-pressure systems.

*Thermal properties*

Figure 4 illustrates how thermal conductivity changes with pressure using DFT calculations, compared with experimental studies. With a pressure range of 0 to 100 GPa, thermal conductivity rises quite linearly from about 30 to 38 $W \cdot m^{-1} \cdot K^{-1}$. This positive trend means higher pressure stiffens atomic vibrations. Phonon group velocity increases, and phonon scattering decreases. With $k=1/3 \cdot C_v \cdot v^2 \cdot \tau$ (where $C_v$ is the specific heat, v is the phonon velocity, and $\tau$ is the phonon relaxation time), thermal conductivity increases.

The nearly parallel DFT and experimental curves show that both methods capture similar physics: pressure favors interatomic coordination by decreasing anharmonicity and phonon scattering. Under the same conditions, no strong phase transition occurs in this range for structural stability, and no obvious pressure-induced phase transition is observed. However, the experimental results are slightly larger than DFT predictions and vary slightly from the theoretical results. This difference, typically less than 1 percent, stems from both computational estimates and experimental conditions.

Therefore, in principle, RTA-based DFT calculations based on the relaxation-time approximation (RTA) would tend to underestimate the thermal conductivity of Boltzmann transport. Instead, they ignore higher-order phonon processes and normal scattering, which redistribute momentum without friction. Furthermore, GGA functionals (e.g., PBE, PBEsol) also slightly underestimate elastic constants and phonon velocities, so they tend to predict lower k values. Underlying numerical constraints (e.g., finite supercell sizes or coarse q-point meshes) can also lead to underestimated values.

At experimental temperatures, slight changes in residual non-hydrostatic stress, microstructure quality, isotopic purity, and radiative heat transfer can bring the measured conductivity closer to expected values. Additional experiments at finite temperatures, anharmonic corrections, and thermal expansion lead to slight changes in phonon lifetimes compared with the 0 K DFT framework. The computational method is based on strong theoretical-experimental agreement, which is important for identifying suitable lattice dynamics in the compression domain.

These subtle discrepancies mainly stem from approximation-induced errors in DFT phonon-transport predictions and small systematic errors in experimental design and calibration, all within the limits of standard scientific methods. This connection also shows that DFT-based prediction systems perform well at predicting thermal properties under pressure. Thus, there is a strong basis for further improvements in this area, such as by introducing temperature-dependent interatomic force constants or by performing iterative Boltzmann transport calculations [27,28].

**Pressure-dependent bulk modulus, Shear modulus, Weng's modulus, and Poisson's ratio with experimental values**

| Pressure (GPa) | Bulk modulus (GPa)-DFT | Shear modulus (GPa) | Weng's modulus (GPa) | Poisson's ratio | Experimental (GPa) [22] |
|---|---|---|---|---|---|
| 0 | 253 | 170 | 410 | 0.22 | 253 |
| 20 | 268 | 180 | 435 | 0.22 | 268 |
| 40 | 285 | 190 | 455 | 0.21 | 280 |
| 60 | 300 | 200 | 475 | 0.21 | 295 |
| 80 | 315 | 210 | 495 | 0.21 | 310 |
| 100 | 330 | 220 | 515 | 0.20 | 320 |

*Optical properties*

Figure 5 presents the absorption edge (in eV) of $Al_2O_3$ at various pressures (e.g., 0–100 GPa) and compares it with DFT results and experimental data [29,30]. However, the absorption edge decreases further with increasing pressure, from about 9.9 eV at 0 GPa to 8.2–8.3 eV at 100 GPa. This results in a large shift of the absorption edge under compression. A reduction in the absorption-edge energy decreases the band gap. Under pressure, the spacing between Al and O atoms in the same plane decreases, increasing orbital overlap and altering the electronic band structure. This reduces the energy gap between the valence and conduction bands. The interband transition between the valence and conduction bands becomes narrower. The clear downward trends observed in DFT, along with experimental results, confirm the systematic effect of pressure on $Al_2O_3$ optical parameters. DFT and experimental data agree well [29,30]. The pressure range is fully explored. The difference between DFT and experimental data is small and consistent. This validates the reliability of the computational approach; DFT also faithfully captures pressure-dependent electronic transitions in $Al_2O_3$.

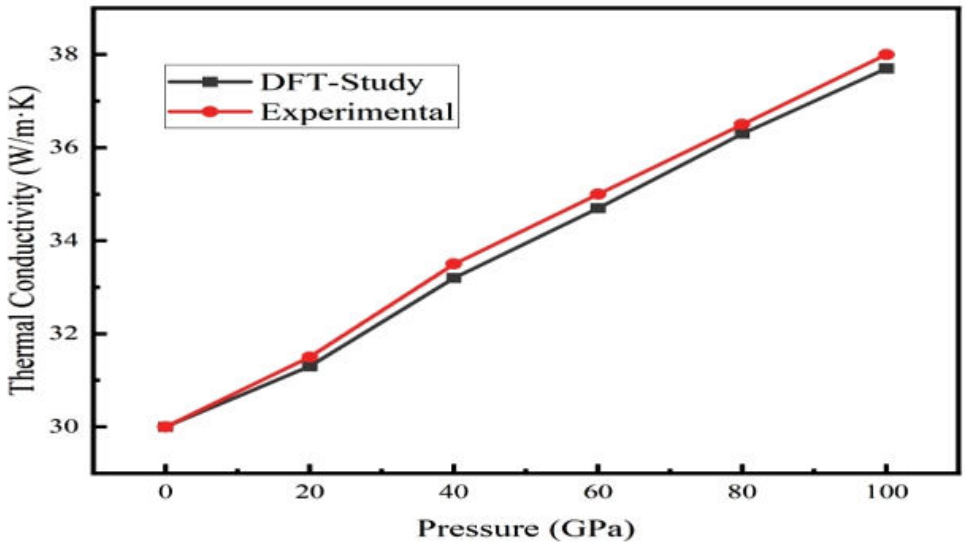



Fig. 4. Variation of thermal conductivity with respect to pressure of $Al_2O_3$ with experimental values [27,28]

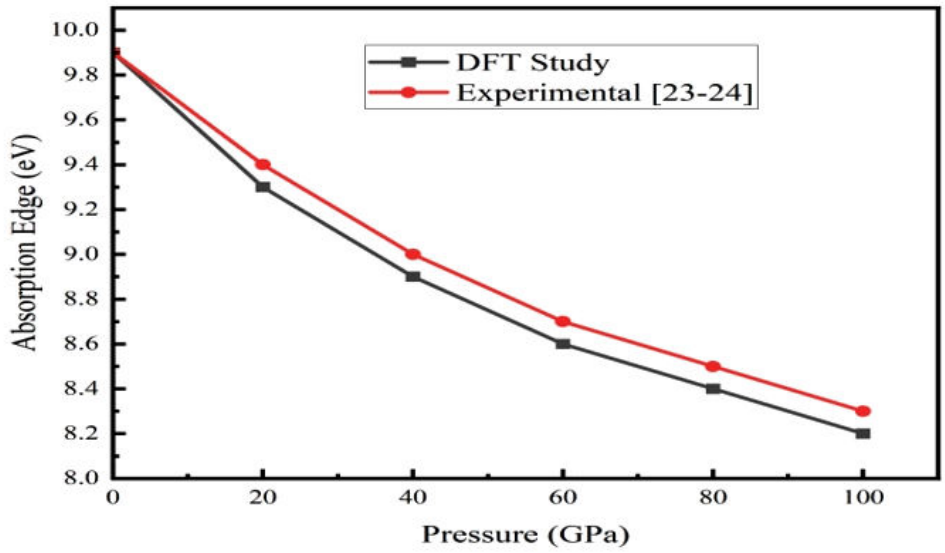



Fig. 5. Pressure-dependent absorption edge of $Al_2O_3$ calculated by DFT with experimental data [29,30]

*Refractive index*

Using bar charts (Fig. 6), this paper shows how the refractive index varies with photon energy (eV) across two pressure regimes: standard pressure (0 GPa) and extreme pressure (100 GPa). The paper provides refractive index values over a photon-energy range of 0–10 eV. In the lower-energy range (0–4 eV), the refractive index is slightly higher at 100 GPa. This suggests that this pressure application enhances light's bending ability, especially at these lower energy levels. At higher photon energies, the refractive-index gap deepens under both pressures.

The refractive index peaks at about 6 eV, and again, the 100 GPa condition (approximately 3.5) surpasses the 0 GPa condition (roughly 3.0). One could argue that high pressure increases the material's responsiveness to electromagnetic radiation in that energy zone. However, it should be noted that it changes after 6 eV. The refractive index at 100 GPa starts to drop more quickly than at 0 GPa. By 8 eV, the high-pressure refractive index drops; at 10 eV, it has nearly given up together, almost kissed up and left it, reaching a refractive index of 1.1.

The refractive index between around 4 and 6 eV is commonly examined for its pressure sensitivity. At its heart, it's about pressure restricting a substance's optical behavior, except at the photon level. Hence, for specific energy ranges, pressure usually increases the refractive index; at higher photon energies, it decreases, presumably due to changes in the material's electronic band structure. These plots show that pressure isn't the only factor – photon energy also plays a major role, and compression causes fine-grained changes in the material's dielectric properties [31,32].

*Absorption coefficient*

Figure 7 shows the relationship between the absorption coefficient and photon energy. It is indeed interesting to compare the response at 0 GPa to 100 GPa. The absorption coefficient is near zero until about 4 eV. This shows little photon absorption in this low-energy region. It becomes more interesting above 4 eV. At low pressure (below 100 GPa), the absorption coefficient increases. Under high pressure, the absorption coefficient is around 5; under normal conditions, it is around 3 at about 6 eV.

The difference increases with photon energy; at 10 eV, the absorption coefficient jumps to almost 29 at 100 GPa, while at 0 GPa it stays close to 18. It is clear that pressure at all these points increases the surface's optical level; higher-energy photons can be absorbed more readily when the surface is compressed. The most likely reason is that high pressure alters the electronic band structure, leading to more electronic transitions than would otherwise be possible.

*Calculation of mechanical properties by the equation of state*

The Murnaghan [33,34] and Srivastava–Pandey [33,34] equations of state (EOS) are expressed as:

$$P = \frac{K_0}{K_0'}\left[\left(\frac{V}{V_0}\right)^{-K_0'} - 1\right], \quad (1)$$

$$P = \left[\frac{K_0}{a^4}(x)^{-4/3}\right] \times \left[\{a^3(1+\xi+\xi^2+\xi^3\right] + \\ + a^2(-3\xi^2 - 2\xi - 1) + \\ + a(6\xi + 2) - 6\}e^{a\xi} - (a^3 - a^2 + 2a - 6), \quad (2)$$

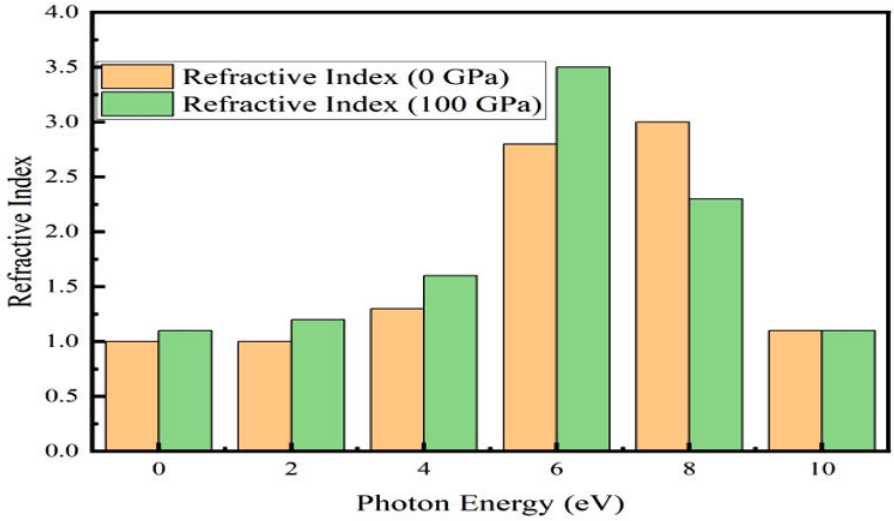



Fig. 6. Refractive index vs. photon energy under various pressures of $Al_2O_3$

where $P$ is the compression-dependent pressure, $K_0$ is the bulk modulus at zero pressure, $K_0'$ is the first-order derivative of the bulk modulus at zero pressure, $x = \frac{V}{V_0}$ is the volume compression, $a = \frac{3K_0' - 8}{3}$, and $\xi = 1 - \frac{V}{V_0}$.

The first volume derivative of the isothermal EOS gives the isothermal bulk modulus ($K_T$) gives [35]:

$$K_T = -V\left(\frac{\partial P}{\partial V}\right)_T . \quad (3)$$

The bulk modulus corresponding to the Murnaghan and Srivastava-Pandey EOS is expressed as [36,37]:

$$K_T = K_0\left(\frac{V}{V_0}\right)^{-K_0'} , \quad (4)$$

$$K_T = K_0\left(\frac{V}{V_0}\right)^{-1/3}(1 + \xi + \xi^2 + \xi^3)\exp(a\xi) + \frac{4}{3}P . \quad (5)$$

Using Eqs. (1) and (2), we can calculate the volume-dependent pressure. Using Eqs. (4) and (5), we can calculate the volume-dependent bulk modulus using the input values. It should be observed that $K_0$=253 and $K_0'$=4 [38].

Figure 8 shows the pressure-volume behavior of a material compared to DFT, Murnaghan's, and Srivastava–Pandey's equations of state. As shown in the plot, pressure declines with increasing volume, indicating that this trend is expected and is also inverse for compressible materials. DFT data points in particular fit both EOS models well, indicating their accuracy. The Murnaghan and Srivastava–Pandey equations follow a similar trajectory and overlap significantly, particularly in the middle volume range. However, at extreme pressures, differences emerge between the EOS and DFT results, suggesting that the EOS is constrained in capturing quantum phenomena across the pressure range. In general, it seems that either EOS model can accurately explain pressure-volume reactions under compression, at least from my perspective.

From Fig. 9, we can observe a clear correlation between the bulk modulus and the volume of the material as we analyze the various methods – the Murnaghan EOS, the Srivastava–Pandey EOS, the DFT calculations, and the experimental results. This reduction in bulk modulus is almost independent of parameter or device size, since the volume increases from ~78 Å$^3$ to ~108 Å$^3$, according to the study. The inverse relationship is not surprising; it shows the material becoming mechanically «softer» as it expands.

However, this aligns with our understanding that pressure falls as volume increases. In addition, the DFT analysis shows that the material is more robust, especially at lower volumes. The Srivastava–Pandey EOS would underestimate the bulk moduli, while the Murnaghan EOS would improve them slightly.

Similarly, the experimental data in source [22] agree strongly with both the DFT predictions and the EOS forecasts. This correlation reinforces the rigor of the theoretical models that we use. The graph illustrates how different EOS models can describe and modify the material's mechanical properties under pressure variation. It shows that, ultimately, both DFT and

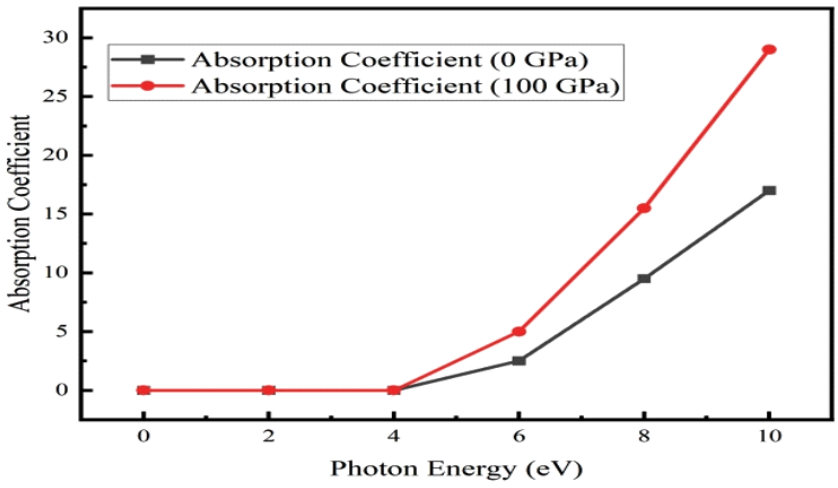



Fig. 7. Variation of absorption coefficient with photon energy at different pressures of $Al_2O_3$

experimental methods are robust and informative for understanding these phenomena.

***Conclusions***

At uniform pressure (similar to that found deep within the Earth), the electronic and optical behavior of aluminum oxide ($Al_2O_3$) will also change at the atomic character level. Here, we study the transition of these properties using Density Functional Theory. In essence, as pressure increases, the bulk modulus and Young's and Shear moduli of the material will rise as well. The volume of the material, however, decreases, and so does Poisson's ratio. The equation of state also confirms this inverse correlation between volume and bulk modulus. So, the band gap decreases with increasing pressure in $Al_2O_3$, an essential aspect of this process, because it reduces the energy electrons need to jump between the two energy levels.

Lower excitation energy directly affects electrical energy transfer and, therefore, interactions with light. Under pressure, the material changes even more spectacularly, beginning to absorb visible light more robustly. Typically transparent, it starts to resonate much more in the visible portion of the spectrum, and this resonance seems more readily associated with pressure-induced changes in the material's band structure. These pressure-induced variations suggest that $Al_2O_3$ is also well suited for pressure-sensitive devices, thereby merging the optics and electronics involved. Mechanical forces that change visible electronics or optics can turn sensors or switches on or off, opening up some promising tech futures.

***Conflict of interest***

The authors declare no known financial interests or personal relationships that could have affected the work presented.

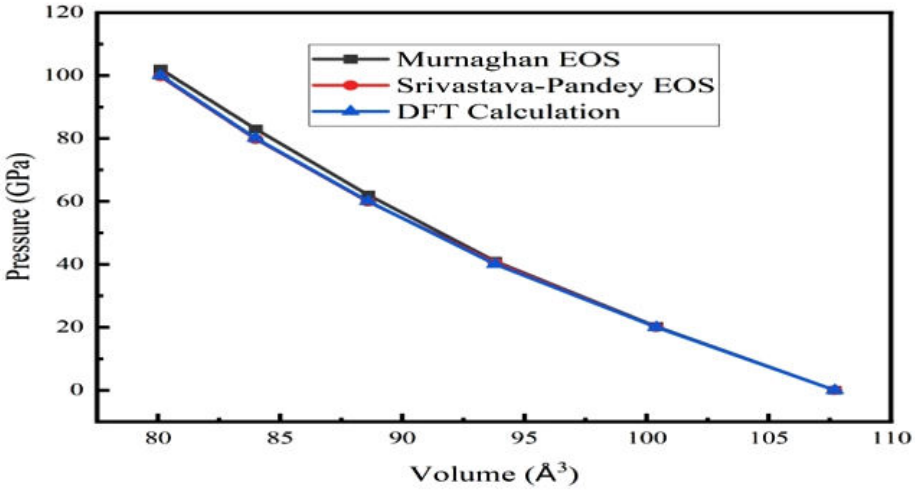



Fig. 8. Variation of pressure with volume of $Al_2O_3$, calculated by DFT and equation of state

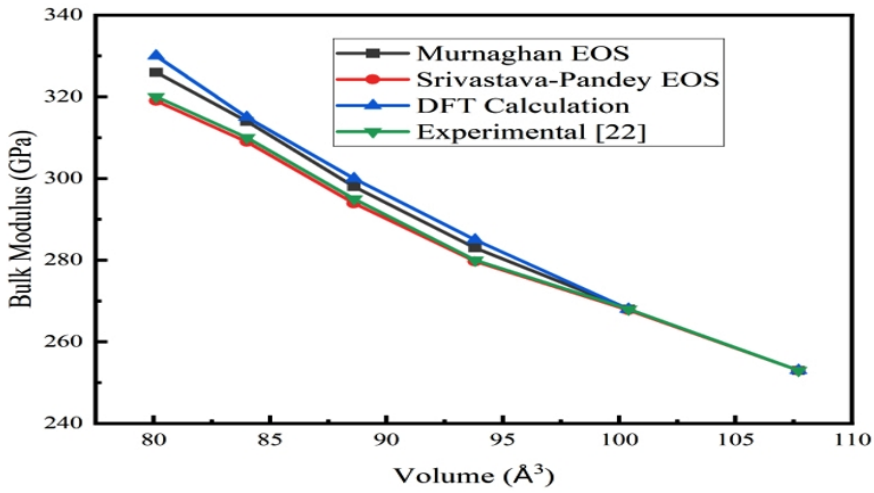



Fig. 9. Variation of bulk modulus with pressure of $Al_2O_3$ calculated by DFT, equation of state with experimental data

## REFERENCES


1. *Handzlik J., Ogonowski J.* DFT study on ethene metathesis proceeding on $MoO_3/Al_2O_3$ catalyst // Ring opening metathesis polymerization and related chemistry. NATO Science Series. – 2002. – Vol.56.

2 *Anti-tumor* drug discovery based on natural product β-elemene anti-tumor mechanisms and structural modification / Bai Z., Yao C., Zhu J., Xie Y., Ye X.Y., Bai R., Xie T. // Molecules. – 2021. – Vol.26. – No. 6. – Art. No. 1499.

3. *Density* functional theory study of chlorine, fluorine, nitrogen, and sulfur doped rutile $TiO_2$ for photocatalytic application / Geldasa F.T., Dejene F.B., Kebede M.A., Hone F.G., Jira E.T. // Sci. Rep. – 2025. – Vol.15. – Art. No. 3390.

4. *Srivastava A.P., Pandey B.K.* Pressure-dependent melting behavior of magnesium orthosilicate: an integrated equation-of-state and first-principles study for Earth's mantle applications // Phys. Chem. Res. – 2026. – Vol.14. – No. 3. – P.449-460.

5. *Srivastava A.P., Pandey B.K.* Analysis of the structural and electronic properties of $TiO_2$ under pressure using density functional theory and equation of state // Comput. Condens. Matter. – 2025. – Vol.44. – Art. No. e01076.

6. *Srivastava A.P., Pandey B.K.* Atomic-level design of doped $TiO_2$ for enhanced lithium storage: a density functional theory approach // J. Electrochem. Soc. – 2025. – Vol.172. – Art. No. 113502.

7. *Katoch S., Chauhan S.S., Kumar V.* A review on genetic algorithm: past, present, and future // Multimed. Tools Appl. – 2021. – Vol.80. – P.8091-8126.

8. *A soft* computing approach to localization in wireless sensor networks / Yun S., Lee J., Chung W., Kim E., Kim S. // Expert. Syst. Appl. – 2009. – Vol.36. – No. 4. – P.7552-7561.

9. Srivastava A.P., Pandey BK. A computational study of pressure-induced melting in $LaFeO_3$: using DFT and a semi-empirical model // Phys. Chem. Res. – 2026. – Vol.14. – No. 1. – P.1-7.

10. *Fabrication*, characterization, and biological evaluation of silymarin nanoparticles against carbon tetrachloride-induced oxidative stress and genotoxicity in rats / Aboshanab M.H., El-Nabarawi M.A., Teaima M.H., El-Nekeety A.A., Abdel-Aziem S.H., Hassan N.S., et al. // Int. J. Pharm. – 2020. – Vol.587. – Art. No. 119639.

11. *Reversion* of malignant phenotypes of human glioblastoma cells by β-elemene through β-catenin-mediated regulation of stemness, differentiation, and epithelial-to-mesenchymal transition-related molecules / Zhu T., Li X., Luo L., Wang X., Li Z., Xie P., et al. // J. Transl. Med. – 2015. – Vol.13. – Art. No. 356.

12. *Thakur S., Thakur I., Kumar R.* A review on synthesized NiO nanoparticles and their utilization for environmental remediation // Inorg. Chem. Commun. – 2025. – Vol.172. – Art. No. 113758.

13. *Revisiting* DFT+U calculations of $TiO_2$ and the effect of the local-projection size / Park K., Raman M., Olatunbosun A.J., Pohlmann J. // AIP Adv. – 2024. – Vol.14. – Art. No. 065114.

14. *Vittadini A., Casarin M., Selloni A.* Chemistry of and on $TiO_2$-anatase surfaces by DFT calculations: a partial review // Theor. Chem. Account. – 2007. – Vol.117. – P.663-671.

15. *Hubbard's* modified density functional theory calculations for the electronic structure and optical properties of carbon-doped anatase $TiO_2$ / Mohamed N.M., Ullah F., Bashiri R., Kait C.F., Saheed M.S.M., Shahid M.U. // Proceedings of the 6th International Conference on Fundamental and Applied Sciences. Springer Proceedings in Complexity. – 2021.

16. *A fundamental* DFT study of anatase ($TiO_2$) doped with 3d transition metals for high photocatalytic activities / Liu X., Li Y., Wei Z., Shi L. // J. Wuhan Univ. Technol.-Mat. Sci. Edit. – 2018. – Vol.33. – P.403-408.

17. *Perdew J.P., Burke K., Ernzerhof M.* Generalized gradient approximation made simple // Phys. Rev. Lett. – 1996. – Vol.77. – No. 18. – P.3865-3868.

18. *Kresse G., Furthmuller J.* Efficient iterative schemes for ab initio total-energy calculations using a plane-wave basis set // Phys. Rev. B. – 1996. – Vol.54. – No. 16. – P.11169-11186.

19. *Multifunctional* properties of $BaTiO_3$ across the cubic–tetragonal phase transition: implications for ferroelectric and electronic applications / Srivastava A.P., Sharma P., Pandey B.K., Mishra A. // J. Inorg. Organomet. Polym. – 2026.

20. *Blanco M.A., Francisco E., Luana V.* GIBBS: isothermal-isobaric thermodynamics of solids from energy curves using a quasi-harmonic Debye model // Comput. Phys. Commun. – 2004. – Vol.158. – No. 1. – P.57-72.

21. *First-principles* methods using CASTEP / Clark S.J., Segall M.D., Pickard C.J., Hasnip P.J., Probert M.I.J., Refson K., et al. // Z. Kristallogr. – 2005. – Vol.220. – No. 5-6. – P.567-570.

22. *Yao Y., Tse J.S.* Electron-phonon coupling in the high-pressure hcp phase of xenon: a first-principles study // Phys. Rev. B. – 2007. – Vol.75. – No. 13. – Art. No. 134104.

23. *Hemley R.J., Mao H.* Anomalous low-frequency excitations in diamond-cell studies of hydrogen at megabar pressures // Phys. Lett. A. – 1992. – Vol.163. – No. 5-6. – P.429-434.

24. *Experimental* study of thermal conductivity at high pressures: implications for the deep Earth's interior / Goncharov A.F., Lobanov S.S., Tan X., Hohensee G.T., Cahill D.G., Lin J.F., et al. // Phys. Earth Planet. Inter. – 2015. – Vol.247. – P.11-16.

25. *Srivastava A.P., Pandey B.K.* First-principles and equation-of-state investigation of pressure-tunable structural, mechanical, thermodynamic, and electronic properties of high-reflecting nano-metal oxides: insights into high-performance optoelectronic and energy applications // Appl. Nanosci. – 2025. – Vol.15. – Art. No. 47.

26. *Filatova E.O., Konashuk A.S.* Interpretation of the change in the band gap of $Al_2O_3$ depending on its crystalline form: connection with different local symmetries // J. Phys. Chem. C. – 2015. – Vol.119. – No. 35. – P.20755-20761.

27. *Thermal* conductivity of materials under pressure / Zhou Y., Dong Z.Y., Hsieh W.P., Goncharov A.F., Chen X.J. // Nat. Rev. Phys. – 2022. – Vol.4. – No. 5. – P.319-335.

28. *Srivastava A.P., Pandey B.K.* Pressure-dependent evolution of $Bi_2Sr_2CaCu_2O_{8+}\delta$: DFT insights for high-pressure superconducting applications // Solid State Commun. – 2025. – Vol.404. – Art. No. 116112.

29. *Zhao W., Sun Z., Alwahabi Z.T.* Emissivity and absorption function measurements of $Al_2O_3$ and SiC particles at elevated temperature for the utilization in concentrated solar receivers // Sol. Energy. – 2020. – Vol.207. – P.183-191.

30. *Visible* light absorption of surface-modified $Al_2O_3$ powders: a comparative DFT and experimental study / Dordevic V., Sredojevic D.N., Dostanic J., Loncarevic D., Ahrenkiel S.P., Svrakic N., et al. // Micropor. Mesopor. Mat. – 2019. – Vol.273. – P.41-49.

31. *Integrated* structural, optical and dielectric analysis of low-loss $\alpha$-$Al_2O_3$ nanoparticles for UV photonic and dielectric applications / Mohamed S.A., Rayan A.M., Abdel Hakeem A.M., Mohamed S.H., Abd El-Rahman A.M., Gad Khater A.E., et al. // Sci. Rep. – 2026. – Vol.16. – Art. No. 14706.

32. *Combined* experimental and DFT study of alumina ($\alpha$-$Al_2O_3$(0001))-supported Fe atoms in the limit of a single atom / Magkoev R.T., Men Y., Behjatmanesh-Ardakani R., Elahifard M., Silaev I.V., Bliev A.P., et al. // Nanomaterials. –2025. – Vol.15. – Art. No. 804.

33. *A new* approach to evaluate pressure of solids at high compression / Srivastava A.P., Pandey B.K., Gupta A.K., Kumar A. // Natl. Acad. Sci. Lett. – 2024. – Vol.47. – P.713-718.

34. *Srivastava A.P., Pandey B.K., Gupta A.K.* Explore the fascinating realm of comparing metal melting curves by applying the equation of state and Lindemann's law // Comput. Condens. Matter. – 2024. – Vol.40. – Art. No. e00952.

35. *Theoretical* prediction of thermoelastic properties of bismuth ferrite by a new approach / Srivastava A.P., Pandey B.K., Gupta A.K., Pandey A.K. // J. Math. Chem. – 2024. – Vol.62. – P.2253-2264.

36. *Sound* velocities of single-crystal MgO to 8 GPa and 1600 K / Chen B., Penwell D., Benedetti L.R., Jeanloz R., Kruger M.B. // Phys. Rev. B. – 2002. – Vol.66. – No. 14. – Art. No. 144101.

37. *Srivastava A.P., Pandey B.K.* Ab initio design of Zr-based bulk metallic glass for high-strength and optical coating applications // Opt. Quant. Electron. – 2025. – Vol.57. – Art. No. 561.

38. *Crystal* structure and equation of state of $MgSiO_3$ perovskite / Vanpeteghem C.B., Zhao J., Angel R.J., Ross N.L., Bolfan-Casanova N. // Geophys. Res. Lett. – 2006. – Vol.33. – Art. No. L03306.

Received 21.10.2025
Revised 12.09.2026
Accepted 06.10.2026
Published 28.10.2026

## ДОСЛІДЖЕННЯ ФІЗИЧНИХ ВЛАСТИВОСТЕЙ $Al_2O_3$ ПІД ТИСКОМ: ДОСЛІДЖЕННЯ ІЗ ЗАСТОСУВАННЯМ МЕТОДІВ DFT ТА РІВНЯНЬ СТАНУ

***Абхай П. Шріваствава, Анод Кумар Сінгх, Рітеш Шріваствава, Харіш Чандра Шріваствава***

За допомогою розрахунків з перших принципів на основі теорії функціонала густини (DFT) у поєднанні з рівняннями стану (EOS) Мурнагана та Шріваствави-Пандея комплексно досліджено вплив тиску на структурні, механічні, теплові та оптичні властивості оксиду алюмінію ($Al_2O_3$). На основі структурної оптимізації підтверджено стабільність корундової фази до 100 ГПа; встановлено зменшення об'єму на 10–15%, а модуль об'ємної пружності збільшується від 253 до 330 ГПа. Ширина забороненої зони зменшується від 9,9 до 8,2 еВ зі зростанням тиску, оскільки електронне перекривання збільшується, а спектр оптичного поглинання, ймовірно, зазнає червоного зсуву; модулі об'ємної, зсувної та Венька також збільшуються, що свідчить про зростання нестисливості. Водночас теплопровідність також дещо збільшується від 30 до 37,7 Вт/(м·К), що може бути пов'язано зі збільшенням фононного розсіювання. Оптичні результати виявляють червоний зсув краю поглинання та чутливий до тиску показник заломлення в діапазоні 4–6 еВ. Узгодження між прогнозами DFT та експериментальними результатами додатково підтверджує точність моделі. Ця узгодженість підтверджує перспективність використання $Al_2O_3$ для оптоелектронних і геофізичних застосувань за високого тиску та забезпечує нове розуміння його електронного й оптичного відгуку під тиском.

**Ключові слова**: теорія функціонала густини; $Al_2O_3$; електронні властивості; оптичні властивості; тиск.

**EXPLORING THE PHYSICAL PROPERTIES OF $Al_2O_3$ UNDER PRESSURE: A STUDY UTILIZING DFT AND EQUATION OF STATE METHODS**

***Abhay P. Srivastava [a, *], Anod Kumar Singh [b], Reetesh Srivastava [c], Harish Chandra Srivastava [d]***

**[a] Department of Humanities and Applied Science, Bansal Institute of Engineering and Technology, Lucknow (UP), India**

**[b] Department of Humanities and Applied Science, School of Management Sciences, Lucknow (UP), India**

**[c] Department of Physics, Nandini Nagar P.G. College, Nawabganj, Gonda (UP), India**

**[d] Munna Lal Inter College, Wazirganj, Budaun (UP), India**

**[*] e-mail: abhay.srivastava831@gmail.com**

Using first-principles density functional theory (DFT) calculations in conjunction with the Murnaghan and Srivastava–Pandey equations of state (EOS), we comprehensively investigate the effect of pressure on the structural, mechanical, thermal, and optical properties of aluminum oxide ($Al_2O_3$). Based on structural optimization, we confirm the stability of the corundum phase up to 100 GPa; we find a 10–15% decrease in volume, and the bulk modulus increases from 253 GPa to 330 GPa. The band gap decreases from 9.9 eV to 8.2 eV with rising pressure, as electronic overlap increases and the optical absorption spectrum is likely to be redshifted; the bulk, shear, and Weng's moduli also increase, indicating greater incompressibility. Meanwhile, the thermal conductivity also increases slightly from 30 W/m·K to 37.7 W/m·K, which can be attributed to the increasing phonon scattering. Optical results reveal a redshift of the absorption edge and a pressure-sensitive refractive index in the 4–6 eV range. The agreement between DFT predictions and experimental results further confirms the model's accuracy. This consistency supports the feasibility of $Al_2O_3$ for optoelectronic and geophysical applications at high pressure and provides new insights into its electronic and optical response under pressure.

**Keywords**: density functional theory; $Al_2O_3$; electronic properties; optical properties; pressure.

**REFERENCES**

1. Handzlik J, Ogonowski J. DFT study on ethene metathesis proceeding on $MoO_3/Al_2O_3$ catalyst. In: Khosravi E, Szymanska-Buzar T, editors. *Ring opening metathesis polymerization and related chemistry. NATO Science Series*. Volume 56. Dordrecht: Springer; 2002. doi: 10.1007/978-94-010-0373-5_41.

2 Bai Z, Yao C, Zhu J, Xie Y, Ye XY, Bai R, Xie T. Anti-tumor drug discovery based on natural product β-elemene anti-tumor mechanisms and structural modification. *Molecules*. 2021; 26(6): 1499. doi: 10.3390/molecules26061499.

3. Geldasa FT, Dejene FB, Kebede MA, Hone FG, Jira ET. Density functional theory study of chlorine, fluorine, nitrogen, and sulfur doped rutile $TiO_2$ for photocatalytic application. *Sci Rep*. 2025; 15: 3390. doi: 10.1038/s41598-024-84316-0.

4. Srivastava AP, Pandey BK. Pressure-dependent melting behavior of magnesium orthosilicate: an integrated equation-of-state and first-principles study for Earth's mantle applications. *Phys Chem Res*. 2026; 14(3): 449-460. doi: 10.22036/pcr.2026.580258.2842.

5. Srivastava AP, Pandey BK. Analysis of the structural and electronic properties of $TiO_2$ under pressure using density functional theory and equation of state. *Comput Condens Matter*. 2025; 44: e01076. doi: 10.1016/j.cocom.2025.e01076.

6. Srivastava AP, Pandey BK. Atomic-level design of doped $TiO_2$ for enhanced lithium storage: a density functional theory approach. *J Electrochem Soc*. 2025; 172: 113502. doi: 10.1149/1945-7111/ae1be1.

7. Katoch S, Chauhan SS, Kumar V. A review on genetic algorithm: past, present, and future. *Multimed Tools Appl*. 2021; 80: 8091-8126. doi: 10.1007/s11042-020-10139-6.

8. Yun S, Lee J, Chung W, Kim E, Kim S. A soft computing approach to localization in wireless sensor networks. *Expert Syst Appl*. 2009; 36(4): 7552-7561. doi: 10.1016/j.eswa.2008.09.064.

9. Srivastava AP, Pandey BK. A computational study of pressure-induced melting in $LaFeO_3$: using DFT and a semi-empirical model. *Phys Chem Res*. 2026; 14(1): 1-7. doi: 10.22036/pcr.2025.537079.2712.

10. Aboshanab MH, El-Nabarawi MA, Teaima MH, El-Nekeety AA, Abdel-Aziem SH, Hassan NS, et al. Fabrication, characterization, and biological evaluation of silymarin nanoparticles against carbon tetrachloride-induced oxidative stress and genotoxicity in rats. *Int J Pharm*. 2020; 587: 119639. doi: 10.1016/j.ijpharm.2020.119639.

11. Zhu T, Li X, Luo L, Wang X, Li Z, Xie P, et al. Reversion of malignant phenotypes of human glioblastoma cells by β-elemene through β-catenin-mediated regulation of stemness, differentiation, and epithelial-to-mesenchymal transition-related molecules. *J Transl Med*. 2015; 13: 356. doi: 10.1186/s12967-015-0727-2.

12. Thakur S, Thakur I, Kumar R. A review on synthesized NiO nanoparticles and their utilization for environmental remediation. *Inorg Chem Commun*. 2025; 172: 113758. doi: 10.1016/j.inoche.2024.113758.

13. Park K, Raman M, Olatunbosun AJ, Pohlmann J. Revisiting DFT+U calculations of $TiO_2$ and the effect of the local-projection size. *AIP Adv*. 2024; 14: 065114. doi: 10.1063/5.0211720.

14. Vittadini A, Casarin M, Selloni A. Chemistry of and on $TiO_2$-anatase surfaces by DFT calculations: a partial review. *Theor Chem Account*. 2007; 117: 663-671. doi: 10.1007/s00214-006-0191-4.

15. Mohamed NM, Ullah F, Bashiri R, Kait CF, Saheed MSM, Shahid MU. Hubbard's modified density functional theory calculations for the electronic structure and optical properties of carbon-doped anatase $TiO_2$. In: Abdul Karim SA, Abd Shukur MF, Fai Kait C, Soleimani H, Sakidin H, editors. *Proceedings of the 6th International Conference on Fundamental and Applied Sciences. Springer Proceedings in Complexity*. Singapore: Springer; 2021. doi: 10.1007/978-981-16-4513-6_32.

16. Liu X, Li Y, Wei Z, Shi L. A fundamental DFT study of anatase ($TiO_2$) doped with 3d transition metals for high photocatalytic activities. *J Wuhan Univ Technol-Mat Sci Edit.* 2018; 33: 403-408. doi: 10.1007/s11595-018-1836-5.

17. Perdew JP, Burke K, Ernzerhof M. Generalized gradient approximation made simple. *Phys Rev Lett.* 1996; 77(18): 3865-3868. doi: 10.1103/PhysRevLett.77.3865.

18. Kresse G, Furthmuller J. Efficient iterative schemes for ab initio total-energy calculations using a plane-wave basis set. *Phys Rev B.* 1996; 54(16): 11169-11186. doi: 10.1103/PhysRevB.54.11169.

19. Srivastava AP, Sharma P, Pandey BK, Mishra A. Multifunctional properties of $BaTiO_3$ across the cubic–tetragonal phase transition: implications for ferroelectric and electronic applications. *J Inorg Organomet Polym*. 2026. doi: 10.1007/s10904-026-04390-x.

20. Blanco MA, Francisco E, Luana V. GIBBS: isothermal-isobaric thermodynamics of solids from energy curves using a quasi-harmonic Debye model. *Comput Phys Commun*. 2004; 158(1): 57-72. doi: 10.1016/j.cpc.2003.10.003.

21. Clark SJ, Segall MD, Pickard CJ, Hasnip PJ, Probert MIJ, Refson K, et al. First-principles methods using CASTEP. *Z Kristallogr*. 2005; 220(5-6): 567-570. doi: 10.1524/zkri.220.5.567.65075.

22. Yao Y, Tse JS. Electron-phonon coupling in the high-pressure hcp phase of xenon: a first-principles study. *Phys Rev B.* 2007; 75(13): 134104. doi: 10.1103/PhysRevB.75.134104.

23. Hemley RJ, Mao H. Anomalous low-frequency excitations in diamond-cell studies of hydrogen at megabar pressures. Phys Lett A. 1992; 163(5-6): 429-434. doi: 10.1016/0375-9601(92)90851-C.

24. Goncharov AF, Lobanov SS, Tan X, Hohensee GT, Cahill DG, Lin JF, et al. Experimental study of thermal conductivity at high pressures: implications for the deep Earth's interior. *Phys Earth Planet Inter.* 2015; 247: 11-16. doi: 10.1016/j.pepi.2015.02.004.

25. Srivastava AP, Pandey BK. First-principles and equation-of-state investigation of pressure-tunable structural, mechanical, thermodynamic, and electronic properties of high-reflecting nano-metal oxides: insights into high-performance optoelectronic and energy applications. *Appl Nanosci.* 2025; 15: 47. doi: 10.1007/s13204-025-03124-8.

26. Filatova EO, Konashuk AS. Interpretation of the change in the band gap of $Al_2O_3$ depending on its crystalline form: connection with different local symmetries. *J Phys Chem C.* 2015; 119(35): 20755-20761. doi: 10.1021/acs.jpcc.5b06843.

27. Zhou Y, Dong ZY, Hsieh WP, Goncharov AF, Chen XJ. Thermal conductivity of materials under pressure. *Nat Rev Phys.* 2022; 4(5): 319-335. doi: 10.1038/s42254-022-00423-9.

28. Srivastava AP, Pandey BK. Pressure-dependent evolution of $Bi_2Sr_2CaCu_2O_{8+}\delta$: DFT insights for high-pressure superconducting applications. *Solid State Commun*. 2025; 404: 116112. doi: 10.1016/j.ssc.2025.116112.

29. Zhao W, Sun Z, Alwahabi ZT. Emissivity and absorption function measurements of $Al_2O_3$ and SiC particles at elevated temperature for the utilization in concentrated solar receivers. *Sol Energy*. 2020; 207: 183-191. doi: 10.1016/j.solener.2020.06.079.

30. Dordevic V, Sredojevic DN, Dostanic J, Loncarevic D, Ahrenkiel SP, Svrakic N, et al. Visible light absorption of surface-modified $Al_2O_3$ powders: a comparative DFT and experimental study. *Micropor Mesopor Mat*. 2019; 273: 41-49. doi: 10.1016/j.micromeso.2018.06.053.

31. Mohamed SA, Rayan AM, Abdel Hakeem AM, Mohamed SH, Abd El-Rahman AM, Gad Khater AE, et al. Integrated structural, optical and dielectric analysis of low-loss $\alpha Al_2O_3$ nanoparticles for UV photonic and dielectric applications. *Sci Rep*. 2026; 16: 14706. doi: 10.1038/s41598-026-50503-4.

32. Magkoev RT, Men Y, Behjatmanesh-Ardakani R, Elahifard M, Silaev IV, Bliev AP, et al. Combined experimental and DFT study of alumina ($\alpha$-$Al_2O_3$(0001))-supported Fe atoms in the limit of a single atom. *Nanomaterials*. 2025; 15: 804. doi: 10.3390/nano15110804.

33. Srivastava AP, Pandey BK, Gupta AK, Kumar A. A new approach to evaluate pressure of solids at high compression. *Natl Acad Sci Lett*. 2024; 47: 713-718. doi: 10.1007/s40009-024-01409-0.

34. Srivastava AP, Pandey BK, Gupta AK. Explore the fascinating realm of comparing metal melting curves by applying the equation of state and Lindemann's law. *Comput Condens Matter*. 2024; 40: e00952. doi: 10.1016/j.cocom.2024.e00952.

35. Srivastava AP, Pandey BK, Gupta AK, Pandey AK. Theoretical prediction of thermoelastic properties of bismuth ferrite by a new approach. *J Math Chem*. 2024; 62: 2253-2264. doi: 10.1007/s10910-024-01647-z.

36. Chen B, Penwell D, Benedetti LR, Jeanloz R, Kruger MB. Sound velocities of single-crystal MgO to 8 GPa and 1600 K. *Phys Rev B*. 2002; 66(14): 144101. doi: 10.1103/PhysRevB.66.14410.

37. Srivastava AP, Pandey BK. Ab initio design of Zr-based bulk metallic glass for high-strength and optical coating applications. *Opt Quant Electron*. 2025; 57: 561. doi: 10.1007/s11082-025-08467-8.

38. Vanpeteghem CB, Zhao J, Angel RJ, Ross NL, Bolfan-Casanova N. Crystal structure and equation of state of $MgSiO_3$ perovskite. *Geophys Res Lett*. 2006; 33: L03306. doi: 10.1029/2005GL024955.